Colloids and Surfaces B: Biointerfaces 184 (2019) 110564

Contents lists available at ScienceDirect

Colloids and Surfaces B: Biointerfaces

journal homepage: www.elsevier.com/locate/colsurfb

Perfluorohexyloctane (F_6H_8) as a delivery agent for cyclosporine A in dry eye syndrome therapy – Langmuir monolayer study complemented with infrared nanospectroscopy

Anna Chachaj-Brekiesz[a,*], Anita Wnętrzak[a], Ewelina Lipiec[b,c], Jan Kobierski[d], Patrycja Dynarowicz-Latka[a]

[a] Faculty of Chemistry, Jagiellonian University, Gronostajowa 2, 30-387 Kraków, Poland
[b] Faculty of Physics, Astronomy and Applied Computer Science, Jagiellonian University, Łojasiewicza 11, 30-348 Kraków, Poland
[c] The Henryk Niewodniczański Institute of Nuclear Physics, Polish Academy of Sciences, Radzikowskiego 152, 31-342 Kraków, Poland
[d] Department of Pharmaceutical Biophysics, Faculty of Pharmacy, Jagiellonian University Medical College, Medyczna 9, 30-688 Kraków, Poland

ARTICLE INFO

Keywords:
LB films
Tear film
Cyclosporine A
Semifluorinated alkanes
AFM-IR

ABSTRACT

One of the key challenges in dry eye syndrome therapy is to find a suitable carrier for immunosuppressant drug – cyclosporine A (CsA) – delivery to the eye. To investigate this issue, herein we present a methodology based on the combined analysis in macro- (Langmuir monolayers), micro- (Brewster angle microscopy) and nanoscale (atomic force microscopy and infrared nano-spectroscopy). The applied approach proves that CsA affects the phospholipid part of the tear film lipid layer by loosening molecular packing. This effect can be reversed by the addition of perfluorohexyloctane (F_6H_8). We have highlighted that F_6H_8 increases the availability of CsA and therefore is appropriate carrier for CsA topical delivery to the eye in the dry eye syndrome. In addition, the applied herein procedure provides a simple, low-cost laboratory tool for preliminary studies involving membrane active pharmaceuticals, preceding *in vivo* tests.

1. Introduction

A disorder in the tear film homeostasis can lead to dry eye syndrome (DES), which is a multifactorial disease of the ocular surface [1]. The tear film stability is ensured by its three layers: mucine, aqueous and lipid. The latter, the tear film lipid layer, TLL, consists of amphiphilic sublayer covered with the external nonpolar film [2]. DES can occur as a result of deficiency of aqueous layer, excessive evaporation of tears (i.e. due to abnormalities in TLL) or both [3]. Epidemiological research has demonstrated that frequency of DES occurrence is within 4.4% to even 50% among middle-aged and elderly people worldwide [4]. Pathomechanism of this disease is complicated and diagnostics is multistage (starting from a detailed patient interview through simple laboratory tests, ending with lipidomic analysis of TLL). Therapy is focused on the recovery of tear film homeostasis and predominantly topical symptomatic treatment is applied [5]. In order to relieve symptoms beyond the limitation of environmental impact and eye hygiene improvement, the following treatments can be applied: artificial tears [6], TLL supplements [7] (e.g. castor oil [8], semifluorinated alkanes [9,10]), steroids [11], macrolidic antibiotics and tetracyclines [12].

Currently, DES is associated with inflammatory diseases very common in autoimmune disorders. Therefore, one of the most effective DES treatments is based on the topical use of cyclosporine A (CsA) – cyclic polypeptide, commonly known for its immunosuppressant properties [13]. Namely, at the receptor level, CsA acts as an inhibitor of interleukin-2 release during the T-cells activation and causes suppression of cell-mediated immune response. As a result, it increases both the production of tears and the density of goblet cells [14,15]. The effectiveness of CsA was confirmed by many biological experiments on animal models [16–18] and in clinical trials [19]. Nowadays, there are several commercially available ocular formulations based on CsA (for

Abbreviations: AFM-IR, infrared nano-spectroscopy; ATR-FTIR, attenuated total reflection Fourier transform infrared spectroscopy; BAM, Brewster angle microscopy; CE, cholesteryl ester; CsA, cyclosporine A; DES, dry eye syndrome; DFT, density functional theory; DPPC, 1,2-dipalmitoyl-sn-glycero-3-phosphocholine; DPPE, 1,2-dipalmitoyl-sn-glycero-3-phosphoethanolamine; F_6H_8, perfluorohexyloctane; LB, Langmuir-Blodgett; OAHFA, O-acyl-ω-hydroxyfatty acid; PCA, principal component analysis; SM, sphingomyelin; TLL, tear film lipid layer; WE, wax ester

* Corresponding author.
E-mail address: chachaj@chemia.uj.edu.pl (A. Chachaj-Brekiesz).

https://doi.org/10.1016/j.colsurfb.2019.110564
Received 12 September 2019; Received in revised form 2 October 2019; Accepted 3 October 2019
Available online 07 October 2019

details, see review [20]).

Limitation of the abovementioned approach to DES therapy is associated with difficulties in CsA delivery to the eye. This is related to both the large molecular size of the peptide and its hydrophobicity. If a disorder occurs in the inner layers of the tear film, the therapeutic substance should be transferred through the outer TLL (consisting mostly of nonpolar lipids), and therefore improving the penetrating properties becomes crucial. This can be achieved, among others, by the selection of an appropriate delivery agent that increases CsA penetration into the eye. Such a delivery agent should be characterized – like CsA – by high hydrophobicity. In addition, it should be chemically inert to the tear film and remain neutral to the eye. Carriers for CsA, which are typically used in ocular formulations, are based on nonpolar lipids, such as castor, corn or olive oil and medium-chain triglycerides. Another applied strategy is to improve CsA solubility in ethanol with non-ionic surfactants, e.g. polyoxyl-40 or polysorbate 80 [20].

Promising delivery agents for CsA can be semifluorinated alkanes, which have been extensively studied in our laboratory [21,22]. These compounds are characterized by unique combination of apolarity and amphiphility. This allows for their easy distribution both in apolar and amphiphilic sublayer of TLL. Preliminary studies have shown that such unique combination of properties ensures CsA dissolution and transfer across apolar waxes to the amphiphilic sublayer of TLL. The results of model studies on animals using perfluorohexyloctane ($F(CF_2)_6(CH_2)_8H$, abbr. F_6H_8) have been found to be promising [23,24]. It should be emphasized that semifluorinated alkanes are neutral to ocular surface and themselves possess a therapeutic effect [9,10]. However, the detailed action mode of CsA and semifluorinated alkanes at the molecular level has not been clarified so far. Therefore this paper is aimed to fulfill this gap.

Disorder in biophysical properties of the tear film observed in dry eye syndrome may result from dysfunctions in amphiphilic sublayer of TLL [5], which - in the normal conditions - forms highly ordered system on the surface of aqueous layer and is isolated from the environment by the nonpolar film. Such systems can be characterized with the Langmuir monolayer technique, which was applied to investigate mechanic properties of films from natural samples of human and animal meibomian gland secretions alone [25,26] as well as treated with pharmaceuticals (i.e. hyaluronic acid [27], Cationorm® [28]), drug preservatives (benzalkonium chloride [27,29,30]) or peptides [31]. Some limitations of this approach should be mentioned, i.e. natural samples can be collected only in sub-milligram quantities (which is insufficient for Langmuir experiments); also they show variable composition depending on individual donors and sample collection protocol [31,32]. The main disadvantage is systematic error based on the assumption that the composition of the tear film lipid layer is reflected in the composition of meibomian gland fluid. As reviewed in [32], the lipid composition of meibum differs significantly from that of tears, especially in the phospholipids content (0.006-0.1 mol% in meibum and 5.4–90 mol % of tear lipids). Therefore amphiphilic phospholipids, which physiological origin remains unknown, should also be taken into consideration as they strikingly influence surface properties of films (for detailed analysis see [33,34]) in contrast to nonpolar lipids [35]. Phospholipid/nonpolar lipids mixtures [33,36,37] as well as phospholipids alone [38–40] were successfully applied as artificial models mimicking tear film lipid layer. Model approach allows to focus on a selected part of the tear film (amphiphilic or apolar sublayer of TLL) and monitor the incorporation of surface active agents. Well-defined system allows to monitor rheological properties of samples and additionally describe molecular interactions.

To obtain a complex picture of *i)* molecular organization, *ii)* variations in surface activity, and *iii)* thermodynamics of the artificial lipid layer of the tear film in the presence of CsA and F_6H_8, we decided to carry out an analysis in *macro-* (thermodynamics of interactions based on the Langmuir monolayer technique), *micro-* (Brewster angle microscopy, BAM) and *nano*scale (atomic force microscopy, AFM and infrared nano-spectroscopy, AFM-IR). As a simplified model of the TLL we considered a mixture of phospholipids, i.e. DPPC:DPPE:SM (in proportion 3:2:2) as it reflects their proportions in natural tears [31,41]. It is worth mentioning that the exact lipid composition of natural TLL still remains unclear, however, apart from phospholipids also O-acyl-ω-hydroxyfatty acids (OAHFAs) and high proportion of nonpolar lipids, such as cholesteryl esters (CEs) and wax esters (WEs) are present [33]. When modeling the TLL we did not take into account nonpolar lipids since stability of the tear film is related to the surface activity of the lipid layer [33]. CEs and WEs have been found to be of low surface activity [42], and although at low surface pressures they can coexist together with phospholipids in the form of a monolayer, at high pressures (corresponding to physiological conditions) they are expelled from the monolayer, forming an overlaying layer [33]. Therefore they do not contribute in any significant way to the surface activity of the lipid layer. The role of OAHFAs in TLL has long been unknown until recent report [43] showing their protective role against evaporation of the tear film, however, their surface activity remains low, similarly to CEs and WEs. Taking all the above into consideration and given that we were interested in receiving a stable system which allows monitoring changes in surface activity and conducting thermodynamic analysis, system composed of amphiphilic phospholipids seems appropriate as a simplified model of the tear film lipid layer.

The results of our experiments allowed to understand the mechanisms responsible for CsA and F_6H_8 therapeutic activity (especially the F_6H_8 role as a delivery agent). Moreover, our methodology can be found useful for further investigations of properties and stability of tear film lipid layer as a part of preliminary research preceding *in vivo* tests.

2. Results and discussion

2.1. Langmuir monolayer study completed with BAM and AFM imaging

Measurements of surface pressure − area (π–A) isotherms are a classical and conventional way of characterizing monolayers stability, phase behavior of molecules in Langmuir films, intermolecular interactions and miscibility between components.

To be able to relate the obtained results to physiological conditions, the experiments should be performed at high surface pressure region (26–30 mN/m [39]) and at temperature of 37 °C. Unfortunately, we could not meet the pressure requirement for film containing CsA and had to conduct experiments (analysis of interactions and floating layers textures as well as the transfer of the films onto a solid substrate) at 15 mN/m, as it was the highest pressure for which the monolayer containing CsA was stable. Due to technical difficulties (high water evaporation at elevated temperatures, disturbances in the operation of electronics and microscope) the experiments were performed at room temperature (20 °C). F_6H_8 alone is not capable for monolayers formation and therefore was excluded from considerations regarding the influence of temperature, CsA was found not to be much sensitive to the change of temperature within the range of 20–30 °C (Fig. S.1 in Appendix A), contrary to phospholipids. However, their surface activity remains high both at lower (20 °C) and higher (above 30 °C) temperature. This proves that temperature plays a minor role in terms of surface activity. Moreover, tear lipid layer needs to maintain its functions within the range of ambient temperatures (20–30 °C) [34], and therefore the exact value of experimental temperature is of low impact in the analysis of our results.

Firstly, in order to check the effect of F_6H_8 on monolayer mimicking TLL, we recorded π–A isotherms for respective multicomponent films with and without F_6H_8 (in proportion of 10, 30 and 50 mol%) (Fig. 1).

The π–A isotherm for phospholipid mixture starts to rise at about 73 $Å^2$/molecule. Upon compression, the surface pressure rises homogeneously until film collapse, which occurs at about 70 mN/m. The additio n of F_6H_8 does not influence isotherms' shape, however, they become shifted toward smaller areas in respect to the model.

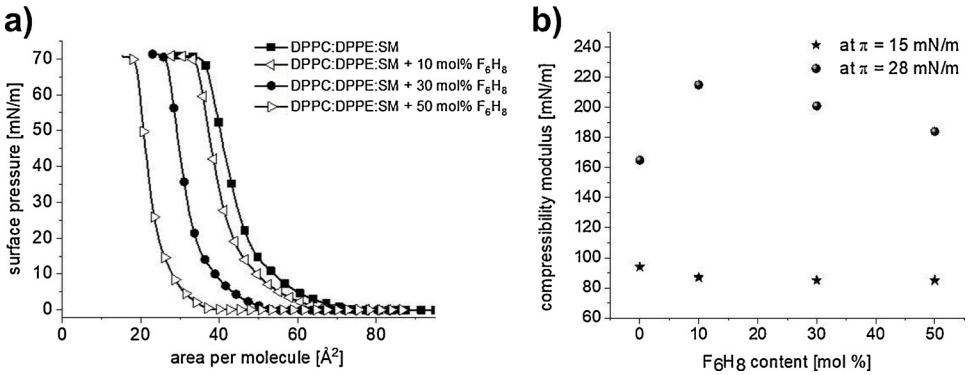

Fig. 1. π–A isotherms of DPPC:DPPE:SM mixed film without and in presence of F_6H_8 (a), C_s^{-1} (at π = 15 and 28 mN/m) as function of F_6H_8 content (b).

Interestingly, the physical states of the investigated monolayers, reflected in compression moduli ($C_s^{-1} = -A\left(\frac{d\pi}{dA}\right)$ [44]) values, are similar ($C_s^{-1} \approx 90$ mN/m for π = 15 mN/m), regardless of the presence and amount of F_6H_8 (see inset in Fig. 1). At 28 mN/m (which is in the middle of the natural tear film surface pressure range [39]) the addition of F_6H_8 slightly increases C_s^{-1} values (the increase is inversely proportional to F_6H_8 content). All the investigated films fall within liquid state. BAM images obtained for systems with different content of F_6H_8 (Fig. S.2 in Appendix A) show almost the same texture of monolayer (oval domains).

In the next step, the investigated monolayers were transferred onto mica and their topography was recorded with AFM. Careful analysis of AFM images acquired from mixed phospholipid system alone and with addition of F_6H_8 (Fig. 2) indicated that both studied surfaces are homogenous and smooth. Profiles extracted along lines marked on AFM images are comparable. These confirms that addition of F_6H_8 does not affect the smoothness and flatness of the surface.

In the next step we have checked changes induced to investigated monolayer by the addition of cyclosporine A. Firstly, CsA in two different proportions (10 and 30 mol%) was added (Fig. 3a). Then, F_6H_8 (30 and 50 mol%, respectively) was added to the system with 30 mol% content of CsA (Fig. 3b).

In mixed phospholipids/CsA systems (Fig. 3a) the presence of CsA causes shifting of the isotherms towards larger areas per molecule, which indicates an increase of intermolecular spacing upon addition of CsA. The slope of the curves is also different in comparison to reference (DPPC/DPPE/SM). In the curve recorded for the system with 10 mol% content of CsA, two collapses are visible: one corresponds exactly to the π_{coll} for pure CsA, and the other one occurs at a higher pressure. Unfortunately, it is impossible to precisely define its value due to its occurrence at a low area (which is out of the moving barrier range). In general, the presence of more than one collapse in the course of an isotherm formed by different components evidences for their immiscibility (total or partial) in a monolayer. For mixtures with 30 mol% content of CsA one can also expect two collapses, however, the lack of second collapse results from the same technical reasons as mentioned above.

The addition of F_6H_8 to the monolayer containing 30 mol% of CsA (Fig. 3b) causes that the isotherms are slightly shifted towards smaller areas per molecule in comparison to the curve registered for the system without F_6H_8. The shift depends on the content of F_6H_8 - the larger the addition is, the smaller area per molecule. Moreover, isotherms for systems containing F_6H_8 are slightly steeper. In the course of these isotherms only one collapse is observed (this may also be due to technical limitations).

In order to provide a detailed description of the effect of CsA and F_6H_8 on the investigated phospholipid mixture, C_s^{-1} values were calculated (at 15 mN/m) and can be seen in Fig. 4a.

The pure DPPC/DPPE/SM mixture and CsA individually form monolayers of the liquid state. The incorporation of CsA causes a

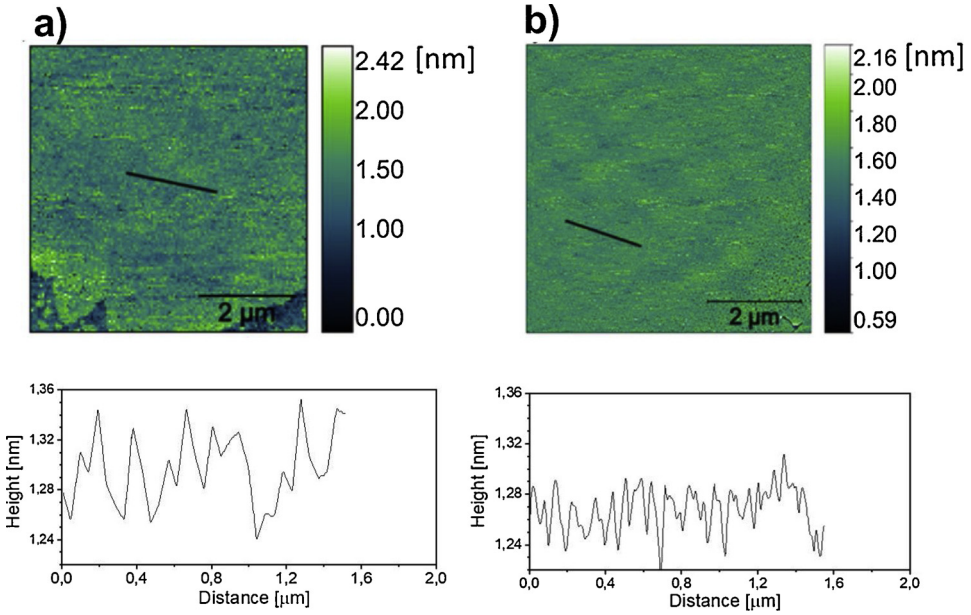

Fig. 2. AFM images of LB films DPPC/DPPE/SM (a) and DPPC/DPPE/SM with addition of 30 mol% F_6H_8(b).

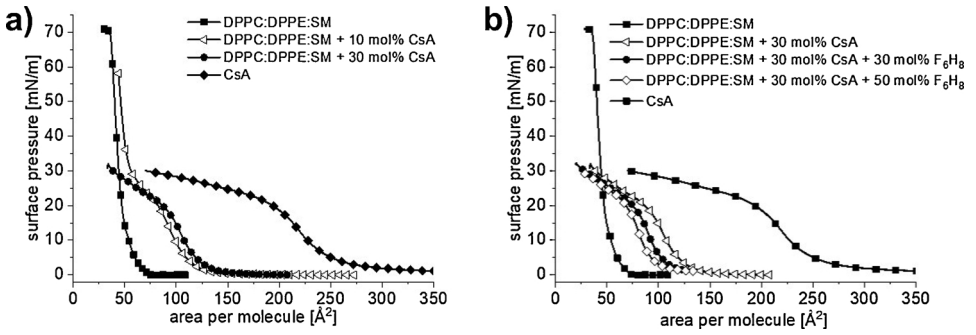

Fig. 3. π–A isotherms of DPPC/DPPE/SM system in the presence of CsA (a) or containing both CsA and F_6H_8 (b).

decrease in film compressibility moduli, especially visible for monolayer with 30% content of CsA. After F_6H_8 addition, C_s^{-1} values increase. It can be connected with the change of molecular ordering in the film.

In Fig. S.3 (see Appendix A) a comparison of BAM images registered at 15 mN/m for pure phospholipid mixture and systems treated with different amount of CsA (with and without presence of F_6H_8) have been shown. As it can be seen, film textures change significantly after CsA incorporation. Domains characteristic for DPPC/DPPE/SM system disappear: only grains with insignificant, blurred borders are observed. The addition of F_6H_8 to the film containing 30 mol% of CsA again changes the texture. For the monolayer poor in F_6H_8, circular domains are observed, while in mixture with high content of F_6H_8, BAM images are more homogenous, however, the texture is not smooth. To analyze the structure of the investigated films more deeply, selected systems were transferred onto mica and AFM topographies were recorded.

Fig. 5 demonstrates AFM images of DPPC/DPPE/SM monolayer with addition of pure CsA (Fig. 5a) and CsA with two different doses of F_6H_8 (Fig. 5b and c). As it can be seen, CsA induces domains formation. In each topography, 1 nm height domains (see profiles) were detected. However, the lateral size of domains was determined by a content of F_6H_8. Our results indicate that an addition of 50 mol% F_6H_8 causes fragmentation of large (4–6 μm diameter) domains induced upon CsA incorporation.

To better understand the role of CsA and F_6H_8, the excess free energy changes (ΔG^{exc}) have been determined (see Fig. 4b). ΔG^{exc} were calculated from the formula $\Delta G^{exc} = N_A \int (A_{12} - (A_1X_1 + A_2X_2))d\pi$ [45], where A_1 is mean molecular area of reference system (DPPC/DPPE/SM with or without addition of F_6H_8), A_2 is mean molecular area of CsA and A_{12} is mean molecular area for DPPC/DPPE/SM film with CsA (with or without addition of F_6H_8), X_2 is molar fraction of CsA and X_1 is molar fraction of reference system ($X_1 = 1\text{-}X_2$). Analysis of the results shows that F_6H_8 influences mutual interactions between CsA and investigated phospholipids mixture. Initially, for the film containing CsA, ΔG^{exc} value is positive, indicating more repulsive interactions between phospholipids and CsA in comparison to reference system (DPPC/DPPE/SM). Positive values may also point to a lower stability of this mixed system. In turn, F_6H_8 stabilizes the system (ΔG^{exc} is negative), indicating that interactions become more attractive (or less repulsive) in comparison to interactions in abovementioned monolayer.

The above-described approach (Langmuir monolayer analysis combined with BAM and AFM) does not provide sufficient information on the composition of the separated phases, therefore further characterization involving nano-spectroscopic method was performed.

2.2. Spectroscopic results

2.2.1. IR spectra in nanoscale compared to bulk samples

To determine chemical composition of different phases in sample of DPPC/DPPE/SM film treated with pharmaceuticals (CsA and F_6H_8), AFM-IR technique [46,47] was applied. Single, floating layers were transferred onto gold coated silica and infrared spectra (in the spectral range 1150–1900 cm^{-1}) were probed at the nanoscale. Places of spectra acquisition were selected based on AFM topography (phase inside and outside domains). Course of representative spectra collected with p polarization was presented in Fig. 6. As it can be seen, spectra recorded from similar places of sample are analogical to each other. Meanwhile, signal from regions localized in domains is different in comparison to that probed from surrounding phase. This suggests differences in chemical composition within and outside domains. At the same time, distribution within each phase is suggested to remain homogeneous. The homogeneity issue will be characterized with PCA

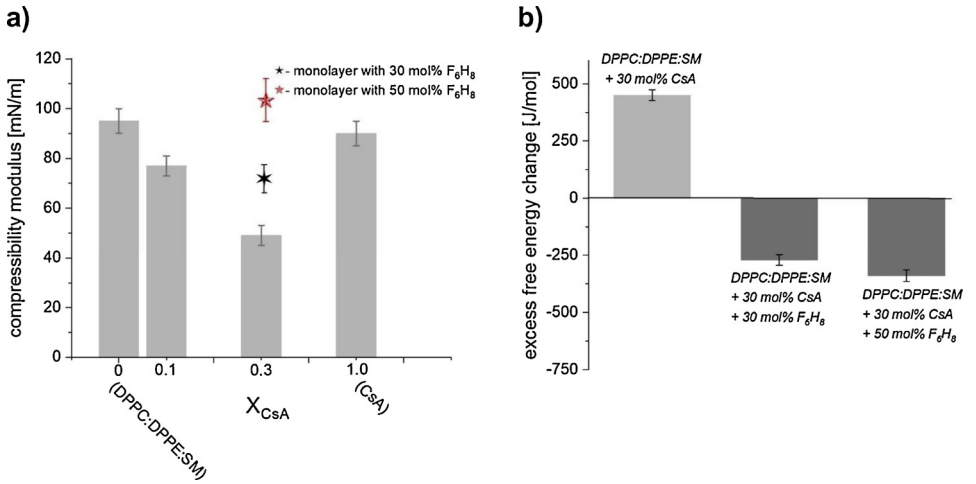

Fig. 4. The effect of CsA and F_6H_8 on DPPC/DPPE/SM film: C_s^{-1} in function of CsA content (a); ΔG^{exc} (b). Values calculated at π = 15 mN/m.

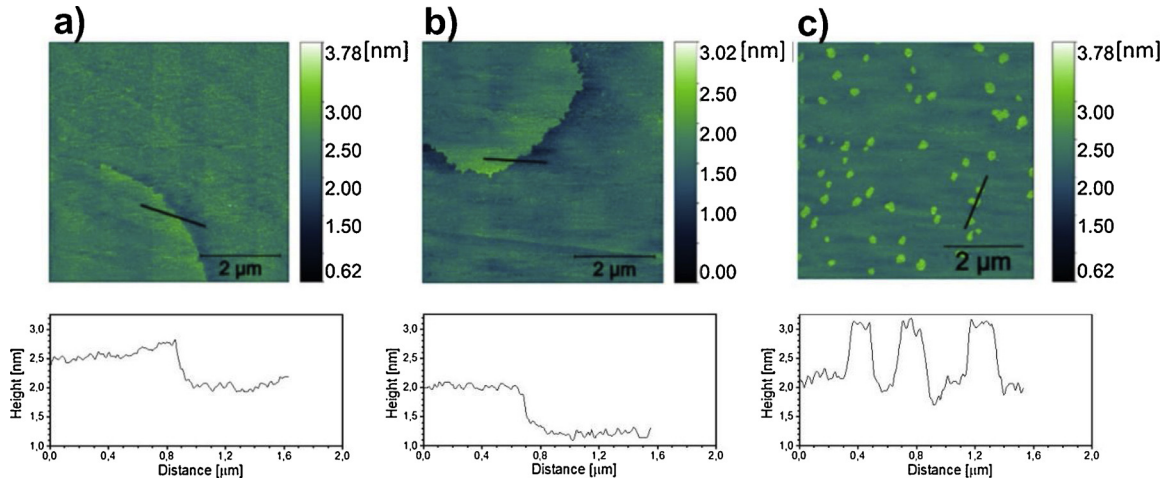

Fig. 5. AFM imaging of DPPC/DPPE/SM monolayer with addition of 30 mol% CsA (a); 30 mol% CsA and 30 mol% F_6H_8 (b); 30 mol% CsA and 50 mol% F_6H_8 (c).

tool (see paragraph 2.2.3).

Further analysis of experimental results obtained from nanoscale required comparison with ATR-FTIR spectra collected from bulk samples. Initially, ATR-FTIR spectra of DPPC/DPPE/SM mixture and DPPC/DPPE/SM treated with CsA and F_6H_8 were compared to AFM-IR spectra (Fig. 6). As it can be seen spectra from nanoscale contain similar bands to those from mixtures in bulk. Differences in mutual intensities of selected bands (nanoscale *vs* bulk) indicate that monolayer samples are more ordered and molecular distribution is not random.

Finally, AFM-IR spectra registered with *p* polarization were systematically compared to ATR-FTIR spectra of bulk substances to notice some important remarks on chemical composition of each phase. Moreover IR spectra of the studied compounds were calculated (for details see Appendix A) and vibrational assignments of observed and calculated frequencies were presented in Table S.1 (Appendix A). This enabled us to select spectral markers of each compound.

In investigated spectral region F_6H_8 absorption is poor with exception of rather wide band with maxima at 1188 and 1234 cm^{-1} attributed to stretching (ν(C–F), ν(C–C)) and bending (wagging ω(C–H), rocking ρ(C–H), twisting τ(C—H)) vibrations. This band is similarly noticeable in spectra probed in nanoscale from inside and surrounding of the domain. Its intensity is almost independent from place of data acquisition therefore it allows to conclude that semifluorinated alkane constitutes matrix for other molecules in film. Polypeptide cyclosporine A in IR spectra shows characteristic band from CH_3 deformational vibrations (at 1410 cm^{-1}), as well as wide intensive bands attributed to amide II (at 1540 cm^{-1}) and amide I (in region 1600–1650 cm^{-1}). Bands observed in nanoscale at 1410 and 1540 cm^{-1} are more intensive and characteristic to spectra collected inside the domains. The increase of intensity of band at 1600–1650 cm^{-1} outside of the domain seems to be confusing, however it can be explained by overlapping with the amide I band characteristic for SM (which concentration is probably greater outside domains). Therefore it can be concluded that cyclosporine A is preferentially accumulated within oval domains. To determine distribution of phospholipids with ester moiety (DPPE and DPPC) diagnostic bands 1702 and 1744 cm^{-1} (arising from ester moieties) were selected. Those bands are more intensive outside domains therefore surrounding phase is enriched in phospholipids.

In the analyzed spectral region there are also bands which originate from all studied compounds and consequently should not be taken into consideration when looking for spectral markers of compounds distribution, however they can suggest degree of molecular packing and ordering. For example, intensive band with maximum at 1480 cm^{-1} is characteristic for all phases of sample as it arises from cumulated

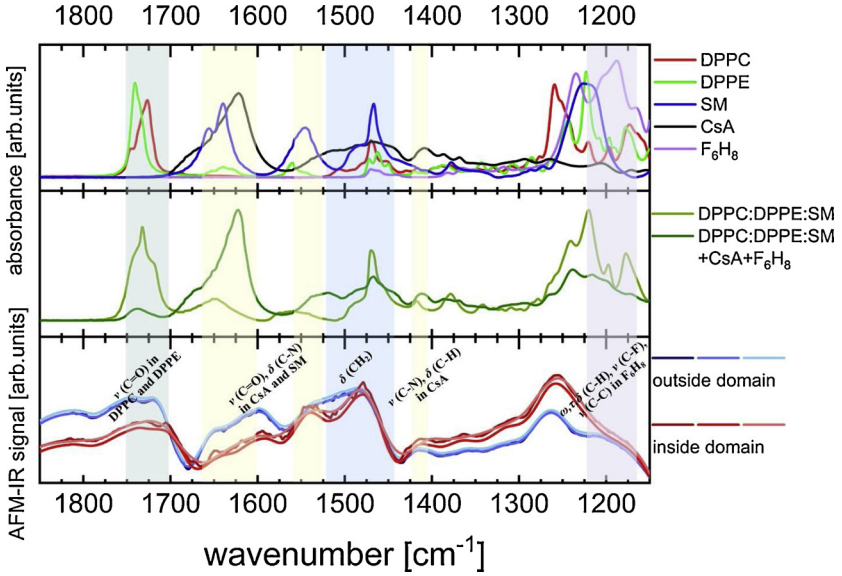

Fig. 6. Comparison of FTIR-ATR spectra of pure compounds in bulk (upper), DPPC/DPPE/SM and DPPC/DPPE/SM treated with CsA and F_6H_8 (middle) with AFM-IR spectra probed with *p*-polarization from DPPC/DPPE/SM film treated with CsA and F_6H_8 (lower).

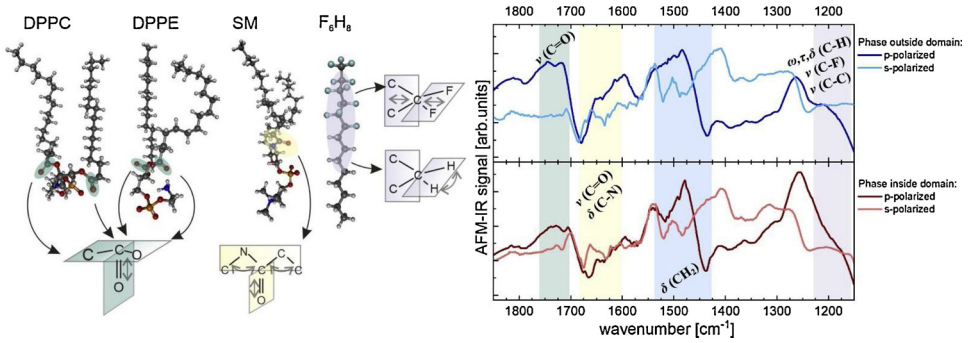

Fig. 7. AFM-IR spectra probed with different polarizations (*s*- and *p*-) from DPPC/DPPE/SM film treated with CsA and F_6H_8: inside (lower panel) and outside (upper panel) the domain together with molecular models.

molecular vibrations of hydrocarbon chains. This band is narrower in case of spectra probed inside the domain therefore it suggests the increase of molecular ordering inside domains.

2.2.2. IR spectra probed with different polarizations

To get a deeper insight into molecular distribution and ordering in the investigated film, additional spectra with different infrared light polarizations (*s* and *p*) were collected. Generally, AFM-IR technique enables observation of different signal intensity from molecular vibrations depending on their orientation to laser polarization [48,49,47]. Namely, the signal is amplified when IR active bonds are oriented in the polarization, otherwise it weakens.

Comparison of selected representative AFM-IR spectra probed from different phases of sample with s and p polarization of infrared light was presented in Fig. 7.

Generally, some differences between spectra from *p*- and *s*-polarization can be noticed. For example, band from hydrocarbon chains (at 1480 cm^{-1}) weakens when s polarization is applied. This observation is in agreement with our previous results [48] and suggests that hydrocarbon chains (from phospholipids and F_6H_8) are predominantly oriented perpendicular to the gold surface. Further evidence for orientation of phospholipids (namely DPPC and DPPE) is partial decrease of absorption intensity at 1702 and 1744 cm^{-1} observed for s polarization. It can be explained with molecular modeling studies which revealed that DPPC ester groups vibrations are perpendicular to substrate surface, while in the case of DPPE they are oriented at 45°. Moreover, the intensity of the abovementioned band is much more noticeable in spectra probed from domains' surrounding. This also confirms that phospholipids are in predominance distributed outside domains.

Additionally, *s*-polarized infrared activates numerous deformation vibrations in F_6H_8 molecule and as a result increased absorption below 1200 cm^{-1} appears. This band is characteristic to spectra collected from both phases (located inside and surrounding domains) which confirms that semifluorinated alkane is uniformly distributed on the surface.

Regarding spectral region attributed to amide I vibrations in SM and CsA in the spectra collected from domains a slight increase in intensity of band at 1665 cm^{-1} for *s*-polarized spectra is observed. It suggests that small quantity of SM is present inside domains. Larger differences can be noticed in the spectra probed from domains' surrounding. For example, absorption in the range 1600-1650 cm^{-1} is increased for *p*-polarization. This observation may provide some information on the origin of this band. Namely, this peak is generated by amide vibrations (from SM and CsA) and in the case of SM can be strongly activated with the polarization direction. The increase of absorption intensity observed for *p*-polarized light suggests that SM molecules are more inclined in monolayer. This results are in agreement with previous studies by GIXD [50], which revealed that SM in other phospholipids environment adopts different orientation (more inclined) compared to films with cholesterol, where it is perpendicular to the surface.

Next, large intensity shift due to different light polarization may be observed regarding spectral bands in 1300-1450 cm^{-1} region, however, due to overlapping of bands from different compounds, this phenomenon does not provide information on molecular orientation.

2.2.3. PCA analysis

Multivariate data analysis here Principal Component Analysis (PCA) is commonly used for spectroscopic data sets in order to reduce large amount of acquired data and explore markers typical for groups of similar spectra. Herein, we have applied PCA to verify spectral variability across nano-metric features observable by AFM. Two PCA models were applied for spectra collected from TLL treated with CsA and F_6H_8 with *s*- and *p*-polarised laser light separately. Fig. 8 demonstrates score plot, which shows the separation of spectra, taken with *p*-polarised light, from the domains and from the neighbouring areas. Scores plot project each spectrum as a single point in the space of new variables called principal components.

This plot confirmed that spectra collected inside and outside domain are distinguishable based on functional groups oriented perpendicular to the surface. Moreover, the distribution of the spectra shows that spectra collected outside the domains are more similar to each other than those acquired inside the domains. This suggests that chemical structure and composition inside the domains is more heterogeneous than inside the surrounding phase. Corresponding loading plot shows spectral differences responsible for the clustering visible on the scores plot. The separation along PC-1, explaining 43% of total variance and it is determined by the band at 1480 cm^{-1} from CH_2 stretching. Loading plot indicates that this band is more intense in the spectra acquired inside the domains (stars located on the positive side of PC-1). This suggests that hydrocarbon chains are more compactly packed inside the domains than outside which confirms presence of CsA (polypeptide with dense molecular structure). The separation along PC-1 is caused also by Amide II band from CsA and SM at 1540 cm^{-1}, characteristic for spectra acquired inside the domains. Another very important factor, which determines the separation along PC-1 is a shift of band attributed to *ν(C–F), ν(C–C), ρ(C–H), τ(C–H)* in F_6H_8 from 1180 cm^{-1} (positive correlation with PC-1) to 1190 cm^{-1} (negative correlation with PC-1). This suggests that F_6H_8 molecule is in slightly different chemical environments inside and outside the domains (inside the domains due to interaction with CsA the vibration energy is different). Negative correlation of PC-1 is observed for Amide I vibrations (1630–1670 cm^{-1}) and band from F_6H_8 (at 1264 cm^{-1}), these bands are characteristic for all spectra collected outside the domains and some spectra acquired inside the domain. Separation along PC-2, which explains 24% of the total variance is also related with Amide II and CH_2, CH_3 deformational modes.

Second PCA model was applied to the spectra acquired with *s*-polarised laser light in order to get deeper insights into nanoscale distribution of chemical bonds oriented parallel to the surface, however no evident separation was observed (Fig. S.4 in Appendix A).

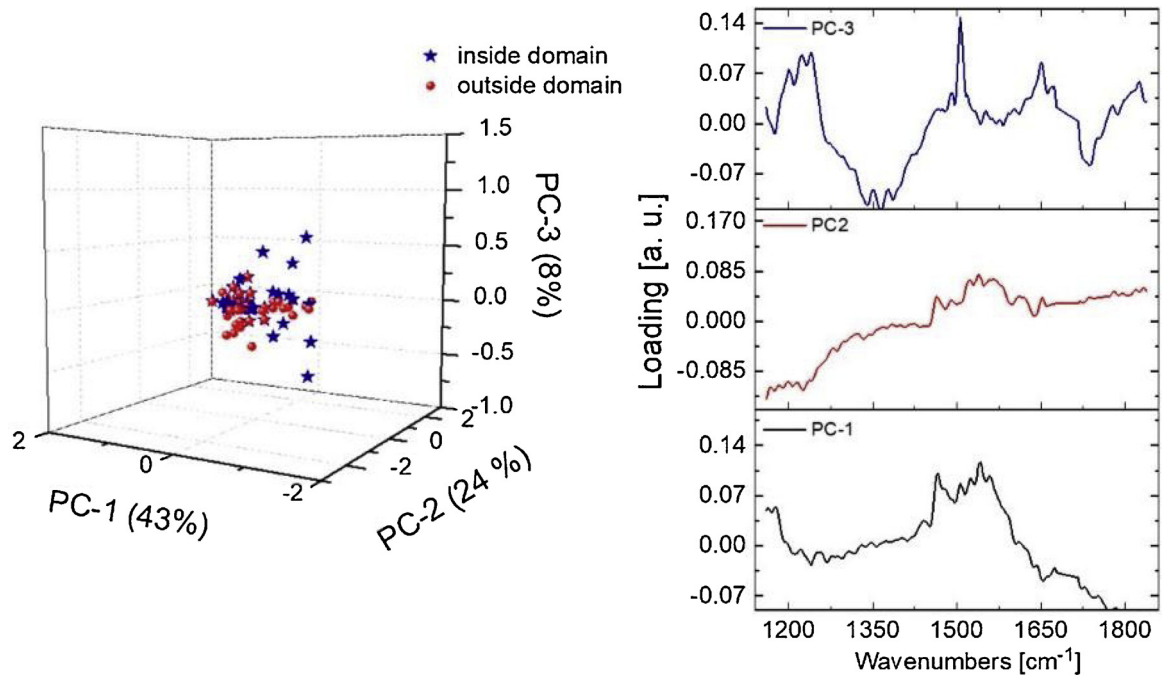

Fig. 8. PCA analysis of AFM-IR spectra collected with *p*-polarised light from the domains and from the neighbouring areas.

3. Conclusions

A variety of experiments conducted on biomimetic self-assembly allowed us to conclude on cyclosporine A and perfluorohexyloctane role in DES therapy. Langmuir monolayer technique complemented with BAM and AFM imaging demonstrated that F_6H_8 (regardless of the dose) does not influence interfacial properties, physical state and texture of DPPC/DPPE/SM mixed film. This confirms that semifluorinated alkane is a good supplement to the tear film lipid layer for use in the DES treatment. Furthermore, our studies revealed that immunosuppressant CsA expandinds DPPC/DPPE/SM monolayer and loosens molecular packing, and this can be reversed by the addition of F_6H_8. In this way, the fluidity of the artificial membrane remains unchanged. This is very important observation and proves that the combination of CsA and semifluorinated alkane can safely be applied in DES therapy. Additionally, we demonstrated that AFM-IR technique provided precise information about molecular distribution and orientation in the investigated biomimetic samples. F_6H_8 increases the availability of CsA, resulting in its more homogeneous distribution within the amphiphilic sublayer of the tear film (as proved by model studies), which is in consistence with previous hypotheses that F_6H_8 increases CsA dispersion [23]. We conclude that synthetic F_6H_8 is a suitable CsA carrier for the treatment of DES. Moreover, multicomponent Langmuir and Langmuir-Blodgett films investigated at ambient laboratory conditions provide a good model to study molecular ordering and packing in the field of drug delivery.

Appendices

Appendix A. Experimental section, Theoretical and experimental IR spectra, Supplementary figures (PDF)

Appendix B. Vibrations of ABA in CsA (GIF)

Appendix C. Vibrations of BMT in CsA (GIF)

Appendix D. Vibrations of MLE in CsA (GIF)

Appendix E. Vibrations of MVA in CsA (GIF)

Appendix F. Vibrations of VAL in CsA (GIF)

Declaration of Competing Interest

The authors declare no conflict of interest

Acknowledgments

The authors are grateful to Professor Wojciech M. Kwiatek (The Henryk Niewodniczański Institute of Nuclear Physics Polish Academy of Sciences) for providing measurement time on nanoIR2 instrument (purchased in frame of the project co-funded by the Małopolska Regional Operational Program Measure 5.1 Krakow Metropolitan Area as an important hub of the European Research Area for 2007-2013, project No. MRPO.05.01.00-12-013/15). This research was supported in part by PL-Grid Infrastructure.

Appendix A. Supplementary data

Supplementary material related to this article can be found, in the online version, at doi:https://doi.org/10.1016/j.colsurfb.2019.110564.

References

[1] J.P. Craig, K.K. Nichols, E.K. Akpek, B. Caffery, H.S. Dua, C.-K. Joo, Z. Liu, J.D. Nelson, J.J. Nichols, K. Tsubota, F. Stapleton, TFOS DEWS II definition and classification report, Ocul. Surf. 15 (2017) 276–283, https://doi.org/10.1016/j.jtos.2017.05.008.

[2] L. Cwiklik, Tear film lipid layer: a molecular level view, Biochim. Biophys. Acta Biomembr. 1858 (2016) 2421–2430, https://doi.org/10.1016/j.bbamem.2016.02.020.

[3] J.L. Gayton, Etiology, prevalence, and treatment of dry eye disease, Clin. Ophthalmol. 3 (2009) 405–412.

[4] M. Uchino, D.A. Schaumberg, Dry eye disease: impact on quality of life and vision, Curr. Ophthalmol. Rep. 1 (2013) 51–57, https://doi.org/10.1007/s40135-013-0009-1.

[5] M.E. Johnson, P.J. Murphy, Changes in the tear film and ocular surface from dry eye syndrome, Prog. Retin. Eye Res. 23 (2004) 449–474, https://doi.org/10.1016/j.preteyeres.2004.04.003.

[6] M.-A. Javadi, S. Feizi, Dry eye syndrome, J. Ophthalmic Vis. Res. 6 (2011) 192–198.

[7] J.S. Garrigue, M. Amrane, M.O. Faure, J.M. Holopainen, L. Tong, Relevance of lipid-based products in the management of dry eye disease, J. Ocul. Pharmacol. Ther. 33 (2017) 647–661, https://doi.org/10.1089/jop.2017.0052.

[8] E. Goto, J. Shimazaki, Y. Monden, Y. Takano, Y. Yagi, S. Shimmura, K. Tsubota, Low-concentration homogenized castor oil eye drops for noninflamed obstructive meibomian gland dysfunction, Ophthalmology 109 (2002) 2030–2035.

[9] P. Steven, A.J. Augustin, G. Geerling, T. Kaercher, F. Kretz, K. Kunert, J. Menzel-Severing, N. Schrage, W. Schrems, S. Krösser, M. Beckert, E.M. Messmer, Semifluorinated alkane eye drops for treatment of dry eye disease due to meibomian gland disease, J. Ocul. Pharmacol. Ther. 33 (2017) 678–685, https://doi.org/10.1089/jop.2017.0042.

[10] P. Steven, D. Scherer, S. Krösser, M. Beckert, C. Cursiefen, T. Kaercher, Semifluorinated alkane eye drops for treatment of dry eye disease—a prospective, multicenter noninterventional study, J. Ocul. Pharmacol. Ther. 31 (2015) 498–503, https://doi.org/10.1089/jop.2015.0048.

[11] A.M. Avunduk, M.C. Avunduk, E.D. Varnell, H.E. Kaufman, The comparison of efficacies of topical corticosteroids and nonsteroidal anti-inflammatory drops on dry eye patients: a clinical and immunocytochemical study, Am. J. Ophthalmol. 136 (2003) 593–602.

[12] J. Frucht-Pery, E. Sagi, I. Hemo, P. Ever-Hadani, Efficacy of doxycycline and tetracycline in ocular rosacea, Am. J. Ophthalmol. 116 (1993) 88–92.

[13] J. Kallen, V. Mikol, V.F.J. Quesniaux, M.D. Walkinshaw, E. Schneider-Scherzer, K. Schörgendorfer, G. Weber, H.G. Fliri, Cyclosporins: recent developments in biosynthesis, pharmacology and biology, and clinical applications, Biotechnology, Wiley-VCH Verlag GmbH, Weinheim, Germany, 2008, pp. 535–591, https://doi.org/10.1002/9783527620890.ch12.

[14] E. Donnenfeld, S.C. Pflugfelder, Topical ophthalmic cyclosporine: pharmacology and clinical uses, Surv. Ophthalmol. 54 (2009) 321–338, https://doi.org/10.1016/j.survophthal.2009.02.002.

[15] S.E. Wilson, H.D. Perry, Long-term resolution of chronic dry eye symptoms and signs after topical cyclosporine treatment, Ophthalmology 114 (2007) 76–79, https://doi.org/10.1016/j.ophtha.2006.05.077.

[16] S. Kilic, K. Kulualp, Efficacy of several therapeutic agents in a murine model of dry eye syndrome, Comp. Med. 66 (2016) 112–118.

[17] S.-J. Hwang, P.R. Karn, H. Kim, H. Kang, B.K. Sun, S.-E. Jin, Supercritical fluid-mediated liposomes containing cyclosporin A for the treatment of dry eye syndrome in a rabbit model: comparative study with the conventional cyclosporin A emulsion, Int. J. Nanomed. 9 (2014) 3791, https://doi.org/10.2147/IJN.S65601.

[18] S.B. Pehlivan, B. Yavuz, S. Çalamak, K. Ulubayram, A. Kaffashi, I. Vural, H.B. Çakmak, M.E. Durgun, E.B. Denkbaş, N. Ünlü, Preparation and in vitro/in vivo evaluation of cyclosporin A-loaded nanodecorated ocular implants for subconjunctival application, J. Pharm. Sci. 104 (2015) 1709–1720, https://doi.org/10.1002/jps.24385.

[19] E.C. Kim, J.-S. Choi, C.-K. Joo, A comparison of vitamin a and cyclosporine a 0.05% eye drops for treatment of dry eye syndrome, Am. J. Ophthalmol. 147 (2009) 206–213, https://doi.org/10.1016/j.ajo.2008.08.015 e3.

[20] F. Lallemand, M. Schmitt, J.-L. Bourges, R. Gurny, S. Benita, J.-S. Garrigue, Cyclosporine A delivery to the eye: a comprehensive review of academic and industrial efforts, Eur. J. Pharm. Biopharm. 117 (2017) 14–28, https://doi.org/10.1016/j.ejpb.2017.03.006.

[21] A. Chachaj-Brekiesz, N. Górska, N. Osiecka, K. Makyła-Juzak, P. Dynarowicz-Łątka, Surface and liquid–crystalline properties of FmHnFm triblock semifluorinated n-alkanes, Mater. Sci. Eng. C 62 (2016) 870–878, https://doi.org/10.1016/j.msec.2016.02.021.

[22] M. Broniatowski, P. Dynarowicz-Łątka, Semifluorinated alkanes — primitive surfactants of fascinating properties, Adv. Colloid Interface Sci. 138 (2008) 63–83, https://doi.org/10.1016/j.cis.2007.11.002.

[23] R.M. Dutescu, C. Panfil, O.M. Merkel, N. Schrage, Semifluorinated alkanes as a liquid drug carrier system for topical ocular drug delivery, Eur. J. Pharm. Biopharm. 88 (2014) 123–128, https://doi.org/10.1016/j.ejpb.2014.05.009.

[24] U. Gehlsen, T. Braun, M. Notara, S. Krösser, P. Steven, A semifluorinated alkane (F4H5) as novel carrier for cyclosporine A: a promising therapeutic and prophylactic option for topical treatment of dry eye, Graefe's Arch. Clin. Exp. Ophthalmol. 255 (2017) 767–775, https://doi.org/10.1007/s00417-016-3572-y.

[25] D.L. Leiske, S.R. Raju, H.A. Ketelson, T.J. Millar, G.G. Fuller, The interfacial viscoelastic properties and structures of human and animal Meibomian lipids, Exp. Eye Res. 90 (2010) 598–604, https://doi.org/10.1016/j.exer.2010.02.004.

[26] P.G. Petrov, J.M. Thompson, I.B.A. Rahman, R.E. Ellis, E.M. Green, F. Miano, C.P. Winlove, Two-dimensional order in mammalian pre-ocular tear film, Exp. Eye Res. 84 (2007) 1140–1146, https://doi.org/10.1016/j.exer.2007.02.012.

[27] G.A. Georgiev, N. Yokoi, S. Ivanova, T. Dimitrov, K. Andreev, R. Krastev, Z. Lalchev, Surface chemistry study of the interactions of hyaluronic acid and benzalkonium chloride with meibomian and corneal cell lipids, Soft Matter 9 (2013) 10841–10856, https://doi.org/10.1039/c3sm51849c.

[28] G.A. Georgiev, N. Yokoi, Y. Nencheva, N. Peev, P. Daull, Surface chemistry interactions of cationorm with films by human meibum and tear film compounds, Int. J. Mol. Sci. 18 (2017), https://doi.org/10.3390/ijms18071558.

[29] G.A. Georgiev, N. Yokoi, K. Koev, E. Kutsarova, S. Ivanova, A. Kyumurkov, A. Jordanova, R. Krastev, Z. Lalchev, Surface chemistry study of the interactions of benzalkonium chloride with films of meibum, corneal cells lipids, and whole tears, Investig. Ophthalmol. Vis. Sci. 52 (2011) 4645–4654, https://doi.org/10.1167/iovs.10-6271.

[30] G.A. Georgiev, N. Yokoi, S. Ivanova, R. Krastev, Z. Lalchev, Surface chemistry study of the interactions of pharmaceutical ingredients with human meibum films, Investig. Ophthalmol. Vis. Sci. 53 (2012) 4605–4615, https://doi.org/10.1167/iovs.12-9907.

[31] T.F. Svitova, M.C. Lin, Dynamic interfacial properties of human tear-lipid films and their interactions with model-tear proteins in vitro, Adv. Colloid Interface Sci. 233 (2016) 4–24, https://doi.org/10.1016/j.cis.2015.12.009.

[32] T.J. Millar, B.S. Schuett, The real reason for having a meibomian lipid layer covering the outer surface of the tear film – a review, Exp. Eye Res. 137 (2015) 125–138, https://doi.org/10.1016/J.EXER.2015.05.002.

[33] A.H. Rantamäki, J. Telenius, A. Koivuniemi, I. Vattulainen, J.M. Holopainen, Lessons from the biophysics of interfaces: lung surfactant and tear fluid, Prog. Retin. Eye Res. 30 (2011) 204–215, https://doi.org/10.1016/j.preteyeres.2011.02.002.

[34] A.H. Rantamäki, J.M. Holopainen, The effect of phospholipids on tear film lipid layer surface activity, Investig. Ophthalmol. Vis. Sci. 58 (2017) 149–154, https://doi.org/10.1167/iovs.16-20468.

[35] P. Kulovesi, A.H. Rantamäki, J.M. Holopainen, Surface properties of artificial tear film lipid layers: effects of wax esters, Investig. Ophthalmol. Vis. Sci. 55 (2014) 4448–4454, https://doi.org/10.1167/iovs.14-14122.

[36] P. Kulovesi, J. Telenius, A. Koivuniemi, G. Brezesinski, I. Vattulainen, J.M. Holopainen, The impact of lipid composition on the stability of the tear fluid lipid layer, Soft Matter 8 (2012) 5826–5834, https://doi.org/10.1039/c2sm25210d.

[37] M. Dwivedi, M. Brinkkötter, R.K. Harishchandra, H.-J. Galla, Biophysical investigations of the structure and function of the tear fluid lipid layers and the effect of ectoine. Part B: artificial lipid films, Biochim. Biophys. Acta Biomembr. 1838 (2014) 2716–2727, https://doi.org/10.1016/J.BBAMEM.2014.05.007.

[38] M.M. Conde, O. Conde, J.M. Trillo, J. Miñones, Approach to knowledge of the interaction between the constituents of contact lenses and ocular tears: mixed monolayers of poly(methyl methacrylate) and dipalmitoyl phosphatidyl choline, Langmuir 27 (2011) 3424–3435, https://doi.org/10.1021/la1051172.

[39] M. Patterson, H.J. Vogel, E.J. Prenner, Biophysical characterization of monofilm model systems composed of selected tear film phospholipids, Biochim. Biophys. Acta Biomembr. 1858 (2016) 403–414, https://doi.org/10.1016/j.bbamem.2015.11.025.

[40] L. Caseli, D. Sousa-Martins, M. Maia, A.A.S. Lima-Filho, E.B. Rodrigues, J. Belfort, An intraocular dye solution based on lutein and zeaxanthin in a surrogate internal limiting membrane model: a Langmuir monolayer study, Colloids Surf. B Biointerfaces 107 (2013) 124–129, https://doi.org/10.1016/j.colsurfb.2013.01.076.

[41] J.T. Saville, Z. Zhao, M.D.P. Willcox, S.J. Blanksby, T.W. Mitchell, Detection and quantification of tear phospholipids and cholesterol in contact lens deposits: the effect of contact lens material and Lens care solution, Investig. Opthalmology Vis. Sci. 51 (2010) 2843, https://doi.org/10.1167/iovs.09-4609.

[42] B.S. Schuett, T.J. Millar, Lipid component contributions to the surface activity of meibomian lipids, Investig. Opthalmol. Vis. Sci. 53 (2012) 7208, https://doi.org/10.1167/iovs.12-10471.

[43] H.C. Bland, J.A. Moilanen, F.S. Ekholm, R.O. Paananen, Investigating the role of specific tear film lipids connected to dry eye syndrome: a study on *O* -Acyl-ω-hydroxy fatty acids and diesters, Langmuir 35 (2019) 3545–3552, https://doi.org/10.1021/acs.langmuir.8b04182.

[44] J.T. Davies, E.K. Rideal, Interfacial Phenomena, Academic Press, 1961.

[45] P. Dynarowicz-Łątka, K. Kita, Molecular interaction in mixed monolayers at the air/water interface, Adv. Colloid Interface Sci. 79 (1999) 1–17, https://doi.org/10.1016/S0001-8686(98)00064-5.

[46] A. Dazzi, C.B. Prater, AFM-IR: technology and applications in nanoscale infrared spectroscopy and chemical imaging, Chem. Rev. 117 (2017) 5146–5173, https://doi.org/10.1021/acs.chemrev.6b00448.

[47] A. Dazzi, C.B. Prater, Q. Hu, D.B. Chase, J.F. Rabolt, C. Marcott, AFM–IR: combining atomic force microscopy and infrared spectroscopy for nanoscale chemical characterization, Appl. Spectrosc. 66 (2012) 1365–1384, https://doi.org/10.1366/12-06804.

[48] E. Lipiec, A. Wnętrzak, A. Chachaj-Brekiesz, W. Kwiatek, P. Dynarowicz-Latka, High-resolution label-free studies of molecular distribution and orientation in ultrathin, multicomponent model membranes with infrared nano-spectroscopy AFM-IR, J. Colloid Interface Sci. 542 (2019) 347–354, https://doi.org/10.1016/j.jcis.2019.02.016.

[49] F. Lu, M. Jin, M.A. Belkin, Tip-enhanced infrared nanospectroscopy via molecular expansion force detection, Nat. Photon. 8 (2014) 307, https://doi.org/10.1038/NPHOTON.2013.373.

[50] P. Wydro, M. Flasiński, M. Broniatowski, Does cholesterol preferentially pack in lipid domains with saturated sphingomyelin over phosphatidylcholine? A comprehensive monolayer study combined with grazing incidence X-ray diffraction and Brewster angle microscopy experiments, J. Colloid Interface Sci. 397 (2013) 122–130, https://doi.org/10.1016/j.jcis.2013.01.060.